

# Gamow-Teller Strengths in $^{26}\text{Mg}$ , $^{76}\text{Ge}$ , $^{82}\text{Se}$ , $^{90}\text{Zr}$ , and $^{92}\text{Zr}$ from the Deformed Quasi-particle RPA (DQRPA)

Eunja Ha\* and Myung-Ki Cheoun †

*Department of Physics, Soongsil University, Seoul 156-743, Korea*

(Dated: December 3, 2024)

We developed the deformed quasi-particle random phase approximation (DQRPA) to describe various properties of deformed nuclei and applied to the evaluation of the Gamow-Teller (GT) transition strength distribution which can be extracted from the experiment of charge exchange reactions (CEXR). Our calculations are started with the single-particle states calculated by the deformed axially symmetric Woods-Saxon potential. Pairing correlations of nucleons, neutron-neutron and proton-proton as well as neutron-proton pairing correlations, are explicitly taken into account at the deformed Bardeen Cooper Schriffer (BCS) theory leading to the quasi-particle concept. The ground state correlations by the many-particle and many-hole mixing states are included by the deformed QRPA. In this work, we use a realistic two-body interaction given by the Brueckner G-matrix based on the Bonn potential to reduce the ambiguity on the nucleon-nucleon interactions inside nuclei. We applied our formalism to the GT transition strengths for  $^{26}\text{Mg}$ ,  $^{76}\text{Ge}$ ,  $^{82}\text{Se}$ ,  $^{90}\text{Zr}$ , and  $^{92}\text{Zr}$ , and compared to available experimental data. The GT strength turns out to be sensitive on the deformation parameter. We suggest most probable deformation parameters for the nuclei by adjusting total GT strength to the experimental data and the Ikeda sum rule, which sum rule is usually thought to be satisfied more or less even under the one-body current approximation without introducing the quenching factor, if high-lying excited states are properly taken into account as in our approach. Most of the experimental GT strength data of the nuclei, in specific, on the high-lying excited states beyond one nucleon threshold are confirmed in our DQRPA by the deformation parameter determined such a way.

---

\* ejha@ssu.ac.kr

† cheoun@ssu.ac.kr

## I. INTRODUCTION

In the core collapsing supernovae (SNe), medium and heavy elements are believed to be produced by the rapid and slow successive neutron capture reaction, dubbed as r-process and s-process, respectively. In these processes, many kinds of unstable neutron-rich nuclei are produced iteratively and decay to more stable nuclei at their turning points in the nuclear chart. These r- and s-processes play vital roles of understanding the nuclear abundances in the cosmos [1]. But, the nucleosynthesis of proton-rich nuclei (p-nuclei), such as  $^{130}\text{La}$ ,  $^{180}\text{Ta}$  and  $^{92}\text{Nb}$ , which located on the neutron-deficient region separately from the stability region, are blocked against these r- and s-processes because of the neighboring stable nuclei. They are believed to be produced exclusively on the neutrino-process, neutrino-induced reactions on related nuclei in core collapse SNe [2–4], where we expect copious numbers of neutrinos from the neutrino sphere at proto-neutron star stage.

Since most of the nuclei produced in the processes are thought to be more or less deformed, we need to explicitly consider effects by the deformation in the nuclear structure and their reactions in the network calculations of the processes.

One more interesting process related to the deformed nuclei may be the rapid rapid proton process (p-process), which is thought to be occurred on the binary star system composed of a neutron star and a companion star, usually white dwarf. Because of the strong gravitation on the neutron star surface, one expects hydrogen rich mass flow from the companion star. Since the high density and low temperature on the neutron star crust makes electrons degenerated, beta decays are usually Pauli blocked by the degeneration, which gives rise to the pycno-reactions [5]. It means that neutron rich nuclei may become stable nuclei, while unstable nuclei may become stable in this situation.

Up to now, main conventional approach to understand the nuclear structure is based on the spherical symmetry. In order to describe neutron-rich nuclei and their relevant nuclear reactions occurred in the nuclear processes, one needs to develop theoretical formalism including explicitly the deformation [6, 7]. Ref. [6] exploited the Nilsson basis to the deformed quasi-particle random phase approximation (DQRPA). But the two-body interaction was derived from the effective separable force. The realistic two-body interaction derived

from the realistic force is firstly exploited at Ref. [7] only with neutron-neutron (nn) and proton-proton (pp) pairing interactions which have only isospin  $T = 1$  and  $J = 0$  interaction. But, to properly describe the deformed nuclei, the  $T = 0$  and  $J = 1$  pairing should be also taken into account because it is intimately related to the deformation by the  $J = 1$  pairing.

In this work, we extend our previous QRPA based on the spherical symmetry [8] to the DQRPA. The spherical QRPA has been exploited as a useful framework for describing the nuclear reactions sensitive on the nuclear structure of medium-heavy and heavy nuclei [9], where, as the mass number increases, the application of the shell model may have actual limits because of tremendous increase of configuration mixing due to the deformation. This paper is organized as follows. In Sec. II, we introduce detailed formalism for the DQRPA and the Gamow-Teller (GT) strength as an application. Numerical results and related discussions are presented at Sec. III. Summary and conclusions are addressed at Sec. IV.

## II. FORMALISM

### A. Total Hamiltonian

We start from the following nuclear Hamiltonian

$$\begin{aligned}
 H &= H_0 + H_{\text{int}} , \\
 H_0 &= \sum_{\alpha\rho_\alpha\alpha'} \epsilon_{\alpha\rho_\alpha\alpha'} c_{\alpha\rho_\alpha\alpha'}^\dagger c_{\alpha\rho_\alpha\alpha'} \quad (\alpha' = p, n) , \\
 H_{\text{int}} &= \sum_{\alpha\beta\gamma\delta\rho_\alpha\rho_\beta\rho_\gamma\rho_\delta, \alpha'\beta'\gamma'\delta'} V_{\alpha\rho_\alpha\alpha'\beta\rho_\beta\beta'\gamma\rho_\gamma\gamma'\delta\rho_\delta\delta'} c_{\alpha\rho_\alpha\alpha'}^\dagger c_{\beta\rho_\beta\beta'}^\dagger c_{\delta\rho_\delta\delta'} c_{\gamma\rho_\gamma\gamma'} ,
 \end{aligned} \tag{1}$$

where the interaction matrix  $V$  is the anti-symmetrized interaction with the Baranger Hamiltonian [10] in which two  $\frac{-1}{2}$  factors, from  $J$  and  $T$  coupling, are included, so that the  $H_{\text{int}}$  in Eq. (1) is equivalent to the usual  $H_{\text{int}} = \frac{1}{4} \sum_{\alpha\beta\gamma\delta\rho_\alpha\rho_\beta\rho_\gamma\rho_\delta, \alpha'\beta'\gamma'\delta'} \tilde{V}_{\alpha\rho_\alpha\alpha'\beta\rho_\beta\beta'\gamma\rho_\gamma\gamma'\delta\rho_\delta\delta'} c_{\alpha\rho_\alpha\alpha'}^\dagger c_{\beta\rho_\beta\beta'}^\dagger c_{\delta\rho_\delta\delta'} c_{\gamma\rho_\gamma\gamma'}$ . The Greek letters denote proton or neutron single particle (s.p.) states with the projection  $\Omega$  of the total angular momentum on the nuclear symmetry axis and the parity  $\pi$ . The projection  $\Omega$  is treated as the only good quantum number in the deformed basis. The  $\rho_\alpha$  ( $\rho_\alpha = \pm 1$ ) is the sign of the angular momentum projection  $\Omega$  of the  $\alpha$  state. The isospin of particles is denoted as a Greek letter with prime, while the isospin of quasi-particles is expressed as a Greek letter with double prime as shown later.

Therefore, the operator  $c_{\alpha\rho\alpha'}^\dagger$  ( $c_{\alpha\rho\alpha'}$ ) in Eq.(1) stands for the usual creation (destruction) operator of the real particle in the state of  $\alpha\rho_\alpha$  with the angular momentum projection  $\Omega_\alpha$  and an isospin  $\alpha'$ , and  $c_{\bar{\alpha}\rho\alpha'} (= (-1)^{j_\alpha+m_\alpha} c_{-\alpha\rho\alpha'})$  is the time reversed operator of  $c_{\alpha\rho\alpha'}$ . Namely our intrinsic states are twofold-degenerate, *i.e.*  $\Omega_\alpha$  state and its time-reversed state  $-\Omega_\alpha$ .  $\epsilon_{\alpha\rho\alpha'}$  means the s.p. state energies.

In cylindrical coordinates, eigenfunctions of a s.p. state and its time-reversed state in deformed Woods-Saxon potential are expressed as follows

$$\begin{aligned} |\alpha\rho_\alpha = +1 \rangle &= \sum_{Nn_z} [b_{Nn_z\Omega_\alpha}^{(+)} |N, n_z, \Lambda_\alpha, \Omega_\alpha = \Lambda_\alpha + 1/2 \rangle \\ &\quad + b_{Nn_z\Omega_\alpha}^{(-)} |N, n_z, \Lambda_\alpha + 1, \Omega_\alpha = \Lambda_\alpha + 1 - 1/2 \rangle], \\ |\alpha\rho_\alpha = -1 \rangle &= \sum_{Nn_z} [b_{Nn_z\Omega_\alpha}^{(+)} |N, n_z, -\Lambda_\alpha, \Omega_\alpha = -\Lambda_\alpha - 1/2 \rangle \\ &\quad - b_{Nn_z\Omega_\alpha}^{(-)} |N, n_z, -\Lambda_\alpha - 1, \Omega_\alpha = -\Lambda_\alpha - 1 + 1/2 \rangle], \end{aligned} \quad (2)$$

where  $N = n_\perp + n_z$  ( $n_\perp = 2n_\rho + \Lambda$ ) is a major shell number, and  $n_z$  and  $n_\rho$  are numbers of nodes on the deformed harmonic oscillator wave functions in  $z$  and  $\rho$  direction, respectively.  $\Lambda$  is the projection of the orbital angular momentum onto the nuclear symmetric axis  $z$ . The coefficients  $b_{Nn_z\Omega}^{(+)}$  and  $b_{Nn_z\Omega}^{(-)}$  are obtained by the eigenvalue equation of the total Hamiltonian in the Nilsson basis. The 2nd terms in Eg. (2) have the same projection  $\Omega_\alpha$  value as the 1st term, but retain another orbital angular momentum because of a flipped spin. Particle model spaces we used depend on the nuclei as shown later on. Single particle spectrum obtained by the deformed Woods Saxon potential is sensitive on the deformation parameter  $\beta_2$  defined as

$$R(\theta) = R_0(1 + \beta_2 Y_{20}(\theta)) , \quad (3)$$

where  $R_0 = 1.2A^{1/3}\text{fm}$  for the sharp-cut radius  $R_0$  [11] and  $Y_{20}$  is spherical harmonics. The customary parameter  $\epsilon = 3(\omega_\perp - \omega_3)/(2\omega_\perp + \omega_3)$  used in the deformed harmonic oscillator is related to as  $\beta_2 \approx (2/3)\sqrt{4\pi/5} \epsilon$  at the leading order. We transform the Hamiltonian represented by real particles in Eq. (1) to the quasi-particle representation through the following Hartree Fock Bogoliubov (HFB) transformation,

$$a_{\alpha\alpha'}^\dagger = \sum_{\beta\beta'} (u_{\alpha\alpha''\beta\beta'} c_{\beta\beta'}^\dagger + v_{\alpha\alpha''\beta\beta'} c_{\bar{\beta}\beta'}), \quad a_{\bar{\alpha}\alpha''} = \sum_{\beta\beta'} (u_{\bar{\alpha}\alpha''\bar{\beta}\beta'}^* c_{\bar{\beta}\beta'} + v_{\bar{\alpha}\alpha''\bar{\beta}\beta'} c_{\beta\beta'}^\dagger). \quad (4)$$

The Hamiltonian, then, can be expressed in terms of the quasi-particles as follows

$$H' = H'_0 + \sum_{\alpha\alpha''} E_{\alpha\alpha''} a_{\alpha\alpha''}^\dagger a_{\alpha\alpha''} + H_{qp.int} . \quad (5)$$

Using the transformation of Eq. (4), finally we obtain the following HFB equation

$$\begin{pmatrix} \epsilon_p - \lambda_p & 0 & \Delta_{p\bar{p}} & \Delta_{p\bar{n}} \\ 0 & \epsilon_n - \lambda_n & \Delta_{n\bar{p}} & \Delta_{n\bar{n}} \\ \Delta_{p\bar{p}} & \Delta_{p\bar{n}} & -\epsilon_p + \lambda_p & 0 \\ \Delta_{n\bar{p}} & \Delta_{n\bar{n}} & 0 & -\epsilon_n + \lambda_n \end{pmatrix}_{\alpha} \begin{pmatrix} u_{\alpha''p} \\ u_{\alpha''n} \\ v_{\alpha''p} \\ v_{\alpha''n} \end{pmatrix}_{\alpha} = E_{\alpha\alpha''} \begin{pmatrix} u_{\alpha''p} \\ u_{\alpha''n} \\ v_{\alpha''p} \\ v_{\alpha''n} \end{pmatrix}_{\alpha}, \quad (6)$$

where  $E_{\alpha\alpha''}$  is the energy of a quasi-particle with the isospin quantum number  $\alpha''$  in the state  $\alpha$ . If we neglect  $\Delta_{np}$ , this equation reduces to the standard Deformed BCS (DBCS) equation.

### B. Spherical and deformed wave functions for a single particle state

Since various mathematical theorems regarding quantum numbers may not be easily used in the deformed basis, it is more convenient to play in the spherical basis. In addition, we exploit the G-matrix based on the Bonn potential in order to pin down plausible ambiguities on the nucleon-nucleon interaction inside a deformed nucleus. Since the G-matrix is calculated on the spherical basis, we need to represent the G-matrix in terms of the deformed basis. Here we present as to how to transform deformed wave functions to spherical wave functions.

The deformed harmonic oscillator wave function,  $|Nn_z\Lambda_\alpha\Omega_\alpha(=\Lambda_\alpha+\Sigma)\rangle = |Nn_z\Lambda_\alpha\rangle |\Sigma\rangle$  in Eq. (2) can be expanded in terms of the spherical harmonic oscillator wave function  $|N_0l\Lambda\rangle |\Sigma\rangle$  as follows

$$\begin{aligned} |Nn_z\Lambda_\alpha\rangle |\Sigma\rangle &= \sum_{N_0=N, N\pm 2, N\pm 4, \dots} \sum_{l=N_0, N_0-2, N_0-4, \dots} A_{Nn_z\Lambda}^{N_0l, n_r=\frac{N_0-l}{2}} |N_0l\Lambda_\alpha\rangle |\Sigma\rangle, \quad (7) \\ |N_0l\Lambda_\alpha\rangle |\Sigma\rangle &= \sum_j C_{l\Lambda_\alpha \frac{1}{2}\Sigma}^{j\Omega_\alpha} |N_0lj\rangle |\Omega_\alpha\rangle. \end{aligned}$$

Here the spatial overlap integral  $A_{Nn_z\Lambda}^{N_0l} = \langle N_0l\Lambda | Nn_z\Lambda \rangle$  is calculated numerically in the spherical coordinate system. Roman letter indicates quantum numbers  $(n_r, l, j)$  of a nucleon state, where  $n_r$  is the radial quantum number and  $l$  is the orbital angular momentum.  $C_{l\Lambda_\alpha \frac{1}{2}\Sigma}^{j\Omega_\alpha}$  is the Clebsch-Gordan coefficient of the coupling of the orbital and spin angular momenta to total angular momentum with the projection  $\Omega_\alpha$ . Therefore, the expansion can be simply

written as

$$|\alpha\Omega_\alpha\rangle = \sum_a B_a^\alpha |a\Omega_\alpha\rangle, \quad (8)$$

with the expansion coefficient summarized as  $B_a^\alpha = \sum_{Nn_z\Sigma} C_{l\Lambda\frac{1}{2}\Sigma}^{j\Omega_\alpha} A_{Nn_z\Lambda}^{N_0l} b_{Nn_z\Sigma}$ .

The DBCS Eq. (6) is solved by using the Brueckner G-matrix calculated from the realistic Bonn CD potential for the nucleon-nucleon interaction in the following way. The pairing potentials  $\Delta_p$ ,  $\Delta_n$  and  $\Delta_{pn}$  in Eq. (6) are calculated as

$$\Delta_{\alpha p \bar{\alpha} p} = -\frac{1}{2} \frac{1}{(2a+1)^{1/2}} \sum_{J,c} g_{\text{pair}}^p (g_{\text{pair}}^n) F_{\alpha a \alpha a}^{J0} F_{\gamma c \gamma c}^{J0} G(aacc, J) (2c+1)^{1/2} (u_{1p_c}^* v_{1p_c} + u_{2p_c}^* v_{2p_c}), \quad (9)$$

where  $F_{\alpha \bar{\alpha} \beta b}^{JK'} = B_a^\alpha B_b^\beta C_{j_\alpha \Omega_\alpha j_\beta \Omega_\beta}^{JK'} (K' = \Omega_\alpha + \Omega_\beta)$  is introduced for the transformation to the deformed basis of G-matrix. Here  $K'$ , which is a projection number of the total angular momentum  $J$  onto the  $z$  axis, is selected  $K' = 0$  at the BCS stage because we consider the pairings of the quasi-particles at  $\alpha$  and  $\bar{\alpha}$  states.  $\Delta_{\alpha n \bar{\alpha} n}$  is the same as Eq. (9) with replacement of  $n$  by  $p$ . In order to renormalize the G-matrix, strength parameters,  $g_{\text{pair}}^p$ ,  $g_{\text{pair}}^n$  and  $g_{\text{pair}}^{pn}$  are multiplied to the G-matrix [8] by adjusting the pairing potentials to the empirical pairing potentials,  $\Delta_p^{\text{emp}}$ ,  $\Delta_n^{\text{emp}}$  and  $\Delta_{pn}^{\text{emp}}$ . The empirical pairing potentials of protons (neutrons) and neutron-proton are evaluated by the following symmetric five term formula for the neighboring nuclei

$$\Delta_p^{\text{emp}} = \frac{1}{8} [M(Z+2, N) - 4M(Z+1, N) + 6M(Z, N) - 4M(Z-1, N) + M(Z-2, N)], \quad (10)$$

$$\Delta_n^{\text{emp}} = \frac{1}{8} [M(Z, N+2) - 4M(Z, N+1) + 6M(Z, N) - 4M(Z, N-1) + M(Z, N-2)], \quad (11)$$

$$\begin{aligned} \Delta_{pn}^{\text{emp}} = & \pm \frac{1}{4} \{ 2[M(Z, N+1) + M(Z, N-1) + M(Z-1, N) + M(Z+1, N)] \\ & - [M(Z+1, N+1) + M(Z-1, N+1) + M(Z-1, N-1) + M(Z+1, N-1)] \\ & - 4M(Z, N) \}, \end{aligned} \quad (12)$$

where  $+$ ( $-$ ) stands for even(odd) mass nuclei. As for masses in Eqs. (10) ~ (12), we use empirical masses. For the neutron-rich nuclei far from the stability region, the masses are still unknown. We, thus, are going to use the values from the extrapolation or the values derived from the liquid-drop model,  $\Delta \approx 12A^{-1/2}\text{MeV}$ . More exact mass measurement of the exotic nuclei from the penning trap [12, 13] are greatly helpful for these empirical parameters.

### C. Description of an excited state by the DQRPA

We take the ground state of a target even-even nucleus as the DBCS vacuum for a quasi-particle. In the following, we show how to generate an excited state in a deformed compound nucleus. Since the deformed nuclei have two different frames, the laboratory and the intrinsic frame, we need to consider the relationship of the two frames. The GT excited state in the intrinsic frame of even-even nuclei, which is described by operating a phonon operator to the BCS vacuum  $\mathcal{Q}_{m,K}^\dagger |QRPA\rangle$ , can be transformed to the wave function in the laboratory frame by using the Wigner function  $\mathcal{D}_{MK}^1(\phi, \theta, \psi)$  as follows

$$\begin{aligned} |1M(K), m\rangle &= \sqrt{\frac{3}{8\pi^2}} [\mathcal{D}_{M-K}^1(\phi, \theta, \psi) \mathcal{Q}_{m,K}^\dagger |QRPA\rangle \quad (\text{for } K=0), \\ |1M(K), m\rangle &= \sqrt{\frac{3}{16\pi^2}} [\mathcal{D}_{MK}^1(\phi, \theta, \psi) \mathcal{Q}_{m,K}^\dagger \\ &\quad + (-1)^{1+K} \mathcal{D}_{M-K}^1(\phi, \theta, \psi) \mathcal{Q}_{m,-K}^\dagger |QRPA\rangle \quad (\text{for } K=\pm 1), \end{aligned} \quad (13)$$

where  $M(K)$  is a projection of the total angular momentum onto the  $z$  (the nuclear symmetry) axis. Of course, the  $K$  is accepted as only a good quantum number in deformed nuclei. The QRPA phonon creation operator  $\mathcal{Q}_{m,K}^\dagger$  acting on the ground state is given as

$$\mathcal{Q}_{m,K}^\dagger = \sum_{\alpha\alpha''\beta\beta''} [X_{(\alpha\alpha''\beta\beta''K)}^m A^\dagger(\alpha\alpha''\beta\beta''K) - Y_{(\alpha\alpha''\beta\beta''K)}^m \tilde{A}(\alpha\alpha''\beta\beta''K)]. \quad (14)$$

with pairing creation and annihilation operators comprising two quasi-particles defined as

$$A^\dagger(\alpha\alpha''\beta\beta''K) = a_{\alpha\alpha''}^\dagger a_{\bar{\beta}\beta''}^\dagger, \quad \tilde{A}(\alpha\alpha''\beta\beta''K) = a_{\beta\beta''} a_{\bar{\alpha}\alpha''}, \quad (15)$$

where bar denotes a time-reversal state for a given state. The quasi-particle pairs in two-particle states,  $\alpha$  and  $\bar{\beta}$ , are chosen by the selection rules  $\Omega_\alpha - \Omega_\beta = K$  and  $\pi_\alpha \pi_\beta = 1$ .

Two-body wave functions in deformed basis are calculated from the spherical basis as follows

$$|\alpha\bar{\beta}\rangle = \sum_{abJ} F_{\alpha a \beta b}^{JK} |ab, JK\rangle, \quad (16)$$

where 2-body wave function in the spherical basis is given as  $|ab, JK\rangle = \sum_J C_{j_a \Omega_a j_b \Omega_b}^{JK} |a\Omega_a\rangle |b\Omega_b\rangle$ , and the transformation coefficient is calculated as  $F_{\alpha a \beta b}^{JK} = B_a^\alpha B_b^\beta (-1)^{j_\beta - \Omega_\beta} C_{j_a \Omega_a j_\beta - \Omega_\beta}^{JK}$  which has a phase factor  $(-1)^{j_\beta - \Omega_\beta}$  arising from the time-reversed states  $\bar{\beta}$ .  $B_a^\alpha$  is defined below Eq.(8).

Our QRPA equation in deformed basis leads to the following form.

$$\begin{pmatrix}
A_{\alpha\beta\gamma\delta}^{1111}(K) & A_{\alpha\beta\gamma\delta}^{1122}(K) & A_{\alpha\beta\gamma\delta}^{1112}(K) & B_{\alpha\beta\gamma\delta}^{1111}(K) & B_{\alpha\beta\gamma\delta}^{1122}(K) & B_{\alpha\beta\gamma\delta}^{1112}(K) \\
A_{\alpha\beta\gamma\delta}^{2211}(K) & A_{\alpha\beta\gamma\delta}^{2222}(K) & A_{\alpha\beta\gamma\delta}^{2212}(K) & B_{\alpha\beta\gamma\delta}^{2211}(K) & B_{\alpha\beta\gamma\delta}^{2222}(K) & B_{\alpha\beta\gamma\delta}^{2212}(K) \\
A_{\alpha\beta\gamma\delta}^{1211}(K) & A_{\alpha\beta\gamma\delta}^{1222}(K) & A_{\alpha\beta\gamma\delta}^{1212}(K) & B_{\alpha\beta\gamma\delta}^{1211}(K) & B_{\alpha\beta\gamma\delta}^{1222}(K) & B_{\alpha\beta\gamma\delta}^{1212}(K) \\
-B_{\alpha\beta\gamma\delta}^{1111}(K) & -B_{\alpha\beta\gamma\delta}^{1122}(K) & -B_{\alpha\beta\gamma\delta}^{1112}(K) & -A_{\alpha\beta\gamma\delta}^{1111}(K) & -A_{\alpha\beta\gamma\delta}^{1122}(K) & -A_{\alpha\beta\gamma\delta}^{1112}(K) \\
-B_{\alpha\beta\gamma\delta}^{2211}(K) & -B_{\alpha\beta\gamma\delta}^{2222}(K) & -B_{\alpha\beta\gamma\delta}^{2212}(K) & -A_{\alpha\beta\gamma\delta}^{2211}(K) & -A_{\alpha\beta\gamma\delta}^{2222}(K) & -A_{\alpha\beta\gamma\delta}^{2212}(K) \\
-B_{\alpha\beta\gamma\delta}^{1211}(K) & -B_{\alpha\beta\gamma\delta}^{1222}(K) & -B_{\alpha\beta\gamma\delta}^{1212}(K) & -A_{\alpha\beta\gamma\delta}^{1211}(K) & -A_{\alpha\beta\gamma\delta}^{1222}(K) & -A_{\alpha\beta\gamma\delta}^{1212}(K)
\end{pmatrix} \quad (17)$$

$$\times \begin{pmatrix} \tilde{X}_{(\gamma 1 \delta 1)K}^m \\ \tilde{X}_{(\gamma 2 \delta 2)K}^m \\ \tilde{X}_{(\gamma 1 \delta 2)K}^m \\ \tilde{Y}_{(\gamma 1 \delta 1)K}^m \\ \tilde{Y}_{(\gamma 2 \delta 2)K}^m \\ \tilde{Y}_{(\gamma 1 \delta 2)K}^m \end{pmatrix} = \hbar \Omega_K^m \begin{pmatrix} \tilde{X}_{(\alpha 1 \beta 1)K}^m \\ \tilde{X}_{(\alpha 2 \beta 2)K}^m \\ \tilde{X}_{(\alpha 1 \beta 2)K}^m \\ \tilde{Y}_{(\alpha 1 \beta 1)K}^m \\ \tilde{Y}_{(\alpha 2 \beta 2)K}^m \\ \tilde{Y}_{(\alpha 1 \beta 2)K}^m \end{pmatrix},$$

where 1 and 2 denote the isospin quantum numbers of protons and neutrons. The amplitudes  $X_{\alpha\alpha''\beta\beta''}$  and  $Y_{\alpha\alpha''\beta\beta''}$ , which stand for forward and backward going amplitudes from state  $\alpha\alpha''$  to  $\beta\beta''$ , are related to  $\tilde{X}_{\alpha\alpha''\beta\beta''} = \sqrt{2}\sigma_{\alpha\alpha''\beta\beta''}X_{\alpha\alpha''\beta\beta''}$  and  $\tilde{Y}_{\alpha\alpha''\beta\beta''} = \sqrt{2}\sigma_{\alpha\alpha''\beta\beta''}Y_{\alpha\alpha''\beta\beta''}$ .  $\sigma_{\alpha\alpha''\beta\beta''} = 1$  if  $\alpha = \beta$  and  $\alpha'' = \beta''$ , otherwise  $\sigma_{\alpha\alpha''\beta\beta''} = \sqrt{2}$  [8]. The A and B matrices are given by

$$\begin{aligned}
A_{\alpha\bar{\beta}, \gamma\bar{\delta}}^{\alpha''\beta'', \gamma''\delta''}(K) = & (E_{\alpha\alpha''} + E_{\beta\beta''})\delta_{\alpha\gamma}\delta_{\alpha''\gamma''}\delta_{\bar{\beta}\bar{\delta}}\delta_{\beta''\delta''} - \sigma_{\alpha\alpha''\bar{\beta}\beta''}\sigma_{\gamma\gamma''\bar{\delta}\delta''} \\
& \times [g_{pp}(u_{\alpha\alpha''}u_{\bar{\beta}\beta''}u_{\gamma\gamma''}u_{\bar{\delta}\delta''} + v_{\alpha\alpha''}v_{\bar{\beta}\beta''}v_{\gamma\gamma''}v_{\bar{\delta}\delta''}) V_{\alpha\bar{\beta}, \gamma\bar{\delta}}^K \\
& + g_{ph}(u_{\alpha\alpha''}v_{\bar{\beta}\beta''}u_{\gamma\gamma''}v_{\bar{\delta}\delta''} + v_{\alpha\alpha''}u_{\bar{\beta}\beta''}v_{\gamma\gamma''}u_{\bar{\delta}\delta''}) V_{\alpha\bar{\delta}, \gamma\bar{\beta}}^K \\
& + g_{ph}(u_{\alpha\alpha''}v_{\bar{\beta}\beta''}v_{\gamma\gamma''}u_{\bar{\delta}\delta''} + v_{\alpha\alpha''}u_{\bar{\beta}\beta''}u_{\gamma\gamma''}v_{\bar{\delta}\delta''}) V_{\alpha\gamma, \bar{\delta}\bar{\beta}}^K],
\end{aligned} \quad (18)$$

$$\begin{aligned}
B_{\alpha\bar{\beta}, \gamma\bar{\delta}}^{\alpha''\beta'', \gamma''\delta''}(K) = & -\sigma_{\alpha\alpha''\bar{\beta}\beta''}\sigma_{\gamma\gamma''\bar{\delta}\delta''} \\
& \times [-g_{pp}(u_{\alpha\alpha''}u_{\bar{\beta}\beta''}v_{\gamma\gamma''}v_{\bar{\delta}\delta''} + v_{\alpha\alpha''}v_{\bar{\beta}\beta''}u_{\gamma\gamma''}u_{\bar{\delta}\delta''}) V_{\alpha\bar{\beta}, \gamma\bar{\delta}}^K \\
& + g_{ph}(u_{\alpha\alpha''}v_{\bar{\beta}\beta''}v_{\gamma\gamma''}u_{\bar{\delta}\delta''} + v_{\alpha\alpha''}u_{\bar{\beta}\beta''}u_{\gamma\gamma''}v_{\bar{\delta}\delta''}) V_{\alpha\bar{\delta}, \gamma\bar{\beta}}^K \\
& + g_{ph}(u_{\alpha\alpha''}v_{\bar{\beta}\beta''}u_{\gamma\gamma''}v_{\bar{\delta}\delta''} + v_{\alpha\alpha''}u_{\bar{\beta}\beta''}v_{\gamma\gamma''}u_{\bar{\delta}\delta''}) V_{\alpha\gamma, \bar{\delta}\bar{\beta}}^K],
\end{aligned} \quad (19)$$



$$\begin{aligned}
V_{\alpha\bar{\beta}, \gamma\bar{\delta}}^K &= \sum_J \sum_{abcd} F_{\alpha a \bar{\beta} b}^{JK} F_{\gamma c \bar{\delta} d}^{JK} G(abcd, J), \\
V_{\alpha\bar{\delta}, \gamma\bar{\beta}}^K &= \sum_J \sum_{abcd} F_{\alpha a \bar{\delta} d}^{JK'} F_{\gamma c \bar{\beta} b}^{JK'} G(adcb, J), \\
V_{\alpha\gamma, \delta\bar{\beta}}^K &= \sum_J \sum_{abcd} F_{\alpha a \gamma c}^{JK} F_{\beta b \bar{\delta} d}^{JK} G(acdb, J).
\end{aligned} \tag{20}$$

where  $F_{\alpha a \bar{\beta} b}^{JK'} = B_a^\alpha B_b^\beta C_{j_\alpha \Omega_\alpha j_\beta \Omega_\beta}^{JK'}$  with non-zero  $K' = \Omega_\alpha + \Omega_\beta$  and  $u$  and  $v$  coefficients are determined from deformed HFB calculation with the pairing strength  $g_{\text{pair}}^n, g_{\text{pair}}^p$  and  $g_{\text{pair}}^{np}$  adjusted to the empirical pairing gaps  $\Delta_{nn}, \Delta_{pp}$  and  $\Delta_{np}$ , respectively.  $E_{\alpha\alpha''}$  indicates the quasi-particle energy of the state  $\alpha$  with the quasi-particle isospin  $\alpha''$ . The  $G(F)$  matrices are two body particle - particle (hole) matrix elements obtained as solutions of the Bethe - Goldstone equation from the Bonn potential [14]. If we do not consider the  $np$  pairing correlations, the A and B matrices can be expressed in the following simple form, which is the same as the those of Saleh [7],

$$\begin{aligned}
A_{\alpha\bar{\beta}, \gamma\bar{\delta}}^{pn, p'n'}(K) &= (E_{\alpha p} + E_{\bar{\beta} n}) \delta_{\alpha\gamma} \delta_{pp'} \delta_{\bar{\beta}\bar{\delta}} \delta_{nn'} \\
&- 2 [g_{pp}(u_{\alpha p} u_{\bar{\beta} n} u_{\gamma p'} u_{\bar{\delta} n'} + v_{\alpha p} v_{\bar{\beta} n} v_{\gamma p'} v_{\bar{\delta} n'}) V_{\alpha\bar{\beta}, \gamma\bar{\delta}}^K \\
&+ g_{ph}(u_{\alpha p} v_{\bar{\beta} n} u_{\gamma p'} v_{\bar{\delta} n'} + v_{\alpha p} u_{\bar{\beta} n} v_{\gamma p'} u_{\bar{\delta} n'}) V_{\alpha\bar{\delta}, \gamma\bar{\beta}}^K],
\end{aligned} \tag{21}$$

$$\begin{aligned}
B_{\alpha\bar{\beta}, \gamma\bar{\delta}}^{pn, p'n'}(K) &= - 2 [-g_{pp}(u_{\alpha p} u_{\bar{\beta} n} v_{\gamma p'} v_{\bar{\delta} n'} + v_{\alpha p} v_{\bar{\beta} n} u_{\gamma p'} u_{\bar{\delta} n'}) V_{\alpha\bar{\beta}, \gamma\bar{\delta}}^K \\
&+ g_{ph}(u_{\alpha p} v_{\bar{\beta} n} v_{\gamma p'} u_{\bar{\delta} n'} + v_{\alpha p} u_{\bar{\beta} n} u_{\gamma p'} v_{\bar{\delta} n'}) V_{\alpha\bar{\delta}, \gamma\bar{\beta}}^K],
\end{aligned} \tag{22}$$

where  $\sigma_{\alpha p \bar{\beta} n} \sigma_{\gamma p' \bar{\delta} n'} = 2$ .

#### D. Description of Gamow-Teller Transition

The  $\beta^\pm$  decay operator,  $\hat{\beta}_{1\mu}^\pm$ , is defined in the intrinsic frame as

$$\hat{\beta}_{1\mu}^- = \sum_{\alpha_p \rho_\alpha \beta_n \rho_\beta} < \alpha_p \rho_\alpha | \tau^+ \sigma_K | \beta_n \rho_\beta > c_p^\dagger \tilde{c}_n, \quad \hat{\beta}_{1\mu}^+ = (\hat{\beta}_{1\mu}^-)^\dagger = (-)^\mu \hat{\beta}_{1, -\mu}^-, \tag{23}$$

in which the  $\hat{\beta}_{1\mu}^\pm$  transition operators are related with those in the laboratory system  $\hat{\beta}_M^\pm$  operator as follows

$$\hat{\beta}_M^\pm = \sum_\mu \mathcal{D}_{M\mu}^1(\phi, \theta, \psi) \hat{\beta}_{1\mu}^\pm. \tag{24}$$

The  $\beta^\pm$  transition amplitudes from the ground state of an initial nucleus to the excited state, the one phonon state in a final nucleus, are expressed by

$$\begin{aligned}
& \langle 1(K), m | \hat{\beta}_K^- | QRPA \rangle \\
&= \sum_{\alpha\alpha'' \rho_\alpha \beta \beta'' \rho_\beta} \mathcal{N}_{\alpha\alpha'' \rho_\alpha \beta \beta'' \rho_\beta} \langle \alpha\alpha'' p \rho_\alpha | \sigma_K | \beta \beta'' n \rho_\beta \rangle [u_{p\alpha\alpha''} v_{n\beta\beta''} X_{\alpha\alpha'' \beta \beta'', K} + v_{p\alpha\alpha''} u_{n\beta\beta''} Y_{\alpha\alpha'' \beta \beta'', K}] \\
& \langle 1(K), m | \hat{\beta}_K^+ | QRPA \rangle \\
&= \sum_{\alpha\alpha'' \rho_\alpha \beta \beta'' \rho_\beta} \mathcal{N}_{\alpha\alpha'' \beta \beta''} \langle \alpha\alpha'' p \rho_\alpha | \sigma_K | \beta \beta'' n \rho_\beta \rangle [u_{p\alpha\alpha''} v_{n\beta\beta''} Y_{\alpha\alpha'' \beta \beta'', K} + v_{p\alpha\alpha''} u_{n\beta\beta''} X_{\alpha\alpha'' \beta \beta'', K}]
\end{aligned} \tag{25}$$

where  $| QRPA \rangle$  denotes the correlated QRPA ground state in the intrinsic frame and the normalization factor is given as  $\mathcal{N}_{\alpha\alpha'' \beta \beta''}(J) = \sqrt{1 - \delta_{\alpha\beta} \delta_{\alpha''\beta''} (-1)^{J+T}} / (1 + \delta_{\alpha\beta} \delta_{\alpha''\beta''})$ . The Wigner functions are disappeared by using the orthogonality of two Wigner functions from the operator and the excited state, respectively. This form is also easily reduced to the results by proton-neutron DQRPA without the  $np$  pairing

$$\begin{aligned}
& \langle 1(K), m | \hat{\beta}_K^- | QRPA \rangle \\
&= \sum_{\alpha_p \rho_\alpha \beta_n \rho_\beta} \langle \alpha_p \rho_\alpha | \tau^+ \sigma_K | \beta_n \rho_\beta \rangle [u_{\alpha_p} v_{\beta_n} X_{\alpha_p \beta_n, K} + v_{\alpha_p} u_{\beta_n} Y_{\alpha_p \beta_n, K}] , \\
& \langle 1(K), m | \hat{\beta}_K^+ | QRPA \rangle \\
&= \sum_{\alpha_p \rho_\alpha \beta_n \rho_\beta} \langle \alpha_p \rho_\alpha | \tau^+ \sigma_K | \beta_n \rho_\beta \rangle [u_{\alpha_p} v_{\beta_n} Y_{\alpha_p \beta_n, K} + v_{\alpha_p} u_{\beta_n} X_{\alpha_p \beta_n, K}].
\end{aligned} \tag{26}$$

Here single particle matrix elements of  $\langle \alpha_p \rho_\alpha | \tau^+ \sigma_K | \beta_n \rho_\beta \rangle$  can be expressed in deformed basis [6],

$$\langle \alpha_p \rho_\alpha | \tau^+ \sigma_{K=0} | \beta_n \rho_\beta \rangle = \delta_{\Omega_p \Omega_n} \rho_\alpha \sum_{Nn_z} [b_{Nn_z \Omega_p}^{(+)} b_{Nn_z \Omega_n}^{(+)} - b_{Nn_z \Omega_p}^{(-)} b_{Nn_z \Omega_n}^{(-)}], \tag{27}$$

$$\begin{aligned}
\langle \alpha_p \rho_\alpha | \tau^+ \sigma_{K=1} | \beta_n \rho_\beta \rangle &= -\sqrt{2} \delta_{\Omega_p \Omega_n + 1} \sum_{Nn_z} b_{Nn_z \Omega_p}^{(+)} b_{Nn_z \Omega_n}^{(-)} \quad (\rho_\alpha = \rho_\beta = +1) \\
&= +\sqrt{2} \delta_{\Omega_p \Omega_n + 1} \sum_{Nn_z} b_{Nn_z \Omega_p}^{(-)} b_{Nn_z \Omega_n}^{(+)} \quad (\rho_\alpha = \rho_\beta = -1) \\
&= -\sqrt{2} \delta_{\Omega_p \frac{1}{2}} \delta_{\Omega_n - \frac{1}{2}} \sum_{Nn_z} b_{Nn_z \Omega_p}^{(+)} b_{Nn_z \Omega_n}^{(+)} \quad (\rho_\alpha = +1, \rho_\beta = -1),
\end{aligned} \tag{28}$$

$$\begin{aligned}
\langle \alpha_p \rho_\alpha | \tau^+ \sigma_{K=-1} | \beta_n \rho_\beta \rangle &= \sqrt{2} \delta_{\Omega_p \Omega_n - 1} \sum_{Nn_z} b_{Nn_z \Omega_p}^{(-)} b_{Nn_z \Omega_n}^{(+)} \quad (\rho_\alpha = \rho_\beta = +1) \\
&= -\sqrt{2} \delta_{\Omega_p \Omega_n - 1} \sum_{Nn_z} b_{Nn_z \Omega_p}^{(+)} b_{Nn_z \Omega_n}^{(-)} \quad (\rho_\alpha = \rho_\beta = -1) \\
&= +\sqrt{2} \delta_{\Omega_p - \frac{1}{2}} \delta_{\Omega_n \frac{1}{2}} \sum_{Nn_z} b_{Nn_z \Omega_p}^{(+)} b_{Nn_z \Omega_n}^{(+)} \quad (\rho_\alpha = +1, \rho_\beta = -1).
\end{aligned} \tag{29}$$

To compare our theoretical results to the experimental data, the  $GT(\mp)$  strength functions and their running sums (total strengths) are calculated as

$$B_{GT}^-(m) = \sum_{K=0,\pm 1} | \langle 1(K), m | \hat{\beta}_K^- | QRPA \rangle |^2, \quad (30)$$

$$B_{GT}^+(m) = \sum_{K=0,\pm 1} | \langle 1(K), m | \hat{\beta}_K^+ | QRPA \rangle |^2,$$

$$S_{GT}^- = \sum_{K=0,\pm 1} \sum_m | \langle 1(K), m | \hat{\beta}_K^- | QRPA \rangle |^2, \quad (31)$$

$$S_{GT}^+ = \sum_{K=0,\pm 1} \sum_m | \langle 1(K), m | \hat{\beta}_K^+ | QRPA \rangle |^2.$$

### E. Ikeda Sum Rule

Numerical results for total  $GT(\pm)$  strengths,  $S_{GT}^-$  and  $S_{GT}^+$ , in Eq. (31) are investigated through the Ikeda sum-rule (ISR), which is known to be satisfied more or less independently of the constructed excited states by any nuclear models,

$$S_{GT}^- - S_{GT}^+ = 3(N - Z). \quad (32)$$

The ISR within the Deformed QRPA, denoted as ISR II, is given by

$$\begin{aligned} & (S_{GT}^- - S_{GT}^+)_{ISR II} \\ &= \sum_{K=0,\pm 1} \sum_m [ | \langle 1(K), m | \hat{\beta}_K^- | QRPA \rangle |^2 - | \langle 1(K), m | \hat{\beta}_K^+ | QRPA \rangle |^2 ] \\ &= \sum_{\alpha_p \rho_\alpha \beta_n \rho_\beta} \sum_{K=0,\pm 1} \sum_m | \langle \alpha_p \rho_\alpha | \tau^+ \sigma_K | \beta_n \rho_\beta \rangle |^2 (u_{\alpha_p}^2 v_{\beta_n}^2 - v_{\alpha_p}^2 u_{\beta_n}^2) [(X_{\alpha_p \beta_n, K}^m)^2 - (Y_{\alpha_p \beta_n, K}^m)^2]. \end{aligned} \quad (33)$$

If we use the closure relation for the excited states, the ISR which we denote as ISR I is shown to be easily calculated as follows

$$\begin{aligned} & (S_{GT}^- - S_{GT}^+)_{ISR I} \\ &= \sum_{\alpha_p \rho_\alpha \beta_n \rho_\beta} \sum_{K=0,\pm 1} | \langle \alpha_p \Omega_p | \tau^+ \sigma_K | \beta_n \Omega_n \rangle |^2 (v_{\beta_n}^2 - v_{\alpha_p}^2). \end{aligned} \quad (34)$$

Since we use the limited particle model space in deformed basis under the one-body current without the  $\Delta$  excitation, the above sum rule is a bit broken, but it may be used to constrain

the deformation parameter  $\beta_2$  in Eq. (3) as shown in our numerical results. On the other hand, the ISR in spherical basis is easily shown to satisfy the ISR as follows

$$\begin{aligned}
S_{GT}^- - S_{GT}^+ &= \sum_{a_p b_n} | \langle a_p | \tau^+ \sigma | b_n \rangle |^2 (v_n^2 - v_p^2) \\
&= \sum_{a_p b_n} (2j_a + 1)(2j_b + 1) \delta_{n_a n_b} \delta_{l_a l_b} \left\{ \begin{matrix} \frac{1}{2} & \frac{1}{2} & 1 \\ j_b & j_a & l_a \end{matrix} \right\}^2 (v_n^2 - v_p^2) \\
&= 3 \sum_{b_n} (2j_b + 1) v_n^2 - 3 \sum_{a_p} (2j_a + 1) v_p^2 = 3(N - Z).
\end{aligned} \tag{35}$$

### III. RESULTS

We calculated the Gamow-Teller strength,  $B_{GT}^\pm$  in Eq. (30), on  $^{26}\text{Mg}$ ,  $^{76}\text{Ge}$ ,  $^{82}\text{Se}$ ,  $^{90}\text{Zr}$ , and  $^{92}\text{Zr}$  within the DQRPA. Those nuclei are selected to represent light, medium, and medium-heavy nuclei, respectively, which have experimental data. The single particle states are used up to  $4\hbar\omega$  for all nuclei, in the spherical limit.

Since the GT strength distribution turns out to be sensitive on the deformation parameter,  $\beta_2$  in Eq.(3), we exploited various values of the deformation parameter,  $|\beta_2| \leq 0.3$ , as the default values. For  $^{26}\text{Mg}$ , we extend the  $\beta_2$  value to  $-0.5$  to keep the consistency with the ISR in Eq.(32). For the pairing interaction, the strength parameters  $g_{\text{pair}}^n$  and  $g_{\text{pair}}^p$  in Eq.(9), which are introduced to renormalize the finite Hilbert model particle space, are adjusted to reproduce the empirical pairing gaps through symmetric five term formula Eqs.(10)-(12) [8]. Corresponding values of the deformation parameter  $\beta_2$ , theoretical and empirical pairing gaps are tabulated in Table I.

It is a remarkable point that theoretical ISR results are so sensitive on the deformation parameter,  $\beta_2$ . It may come from the following facts. The single particle state energies adopted from the deformed Woods Saxon potential naturally depends on the parameter  $\beta_2$ . The deformation of nuclei may be conjectured to come from macroscopic phenomena, for example, the core polarization, the high spin states and so on. Microscopic reasons may be traced to the tensor force in nucleon-nucleon interaction, which is known to account for the shell evolution according to the recent systematic shell model calculations [15, 16]. For example,  $T = 0$ ,  $J = 1$  pairing, which is associated with the  $^3S_0$  tensor force, may lead to the deformation compared to the spherical  $T = 1$ ,  $J = 0$  pairing. Therefore, the deformation parameters adopted in this work may include implicitly and effectively such effects, because

the single particle states from the deformed Wood Saxon potential show a strong dependence on the  $\beta_2$  [17].

The deformation parameter  $\beta_2$  may help us to conjecture the nuclear shape through the intrinsic quadrupole moment,  $Q = \sqrt{16\pi/5}(3/4\pi)AR_0^2\beta_2$ , where  $R_0 = 1.2A^{1/3}\text{fm}$  for the sharp-cut radius  $R_0$  [18, 19]. In experimental side, the deformation parameter  $\beta_2$  can be extracted from the E2 transition probability,  $Q = \sqrt{16\pi B(E2)/5e^2}$ . Since we do not have yet enough E2 data to be exploited in the nuclei considered here to our knowledge, we refer to theoretical results by the relativistic mean field theory (RMF) [20]. But the sign of the  $\beta_2$  is sometimes still uncertain and also the coexistence of prolate and oblate shapes are also possible. In this work, such coexistence and  $\beta_4$  deformation are not taken into account.

In the DQRPA stage, we have taken the particle-hole and particle-particle strength parameters,  $g_{ph}$  and  $g_{pp}$  in Eqs.(18)-(19) as 1.0 for for the five nuclei. Actually  $g_{ph}$  might be determined from the Gamow Teller Giant Resonance (GTGR), while fine tuning of  $g_{pp}$  are usually performed for the double beta decay [8].

In this work, we fix them because the GT strengths are not so sensitive on the values. Since the nuclei considered here are expected to have large energy gaps between proton and neutron spaces, we considered only the  $nn$  and  $pp$  pairing correlation although the formalism is presented generally. For example, in the neutron-rich nuclei of importance in the r-process, the  $np$  pairing may not contribute so much. But for the p-process, the  $np$  pairing could be more important than the neutron-rich nuclei because of the adjacent energy gaps of protons and neutrons. The calculations for the neutron-deficient nuclei in p-process are in progress.

In the following figures, we show the GT strength distribution in terms of the  $\beta_2$  parameter, as a function of excited energy of parent nucleus. Therefore, experimental data, which were usually measured w.r.t. the the ground state of daughter nuclei, are presented by subtracting the empirical Q values from the measured data.

In Figs. 1 and 2, we show the GT strength distribution for  $^{26}\text{Mg}$  as a function of the excitation energy  $E_{ex}$  w.r.t.  $^{26}\text{Mg}$  with various deformation parameters  $\beta_2$  in our DQRPA scheme. The excited states of daughter nucleus  $^{26}\text{Al}$  are calculated from the ground state of the parent nucleus  $^{26}\text{Mg}$  as the eigenvalues of the DQRPA in Eq. (17). The uppermost two panels in Figs. 1 and 2 show the experimental  $B(\text{GT}^-)$  data taken form Ref. [21], which were extracted from  $^{26}\text{Mg}(^3\text{He},t)$  reactions at 140 MeV/nucleon and showed an interesting peak on high-lying GT excited states around 15 MeV.

Results of the  $B(GT^-)$  for prolate ( $\beta_2 = 0 \sim 0.3$ ) and oblate shapes ( $\beta_2 = -0.1 \sim -0.5$ ) are shown in Figs.1 and 2, respectively. In each panel, the  $\beta_2$  value and the ISR results, (ISR I, ISR II) in Eqs.(34) and (33), are indicated. In general, GT strengths are a bit scattered from the low-lying states to the high-lying states with the increase of the deformation. But prolate results in Fig.1 do not show the strength around 15 MeV. Therefore, our results for  $^{26}\text{Mg}$  predict oblate deformation about  $\beta_2 = -0.3 \sim -0.5$  as shown in (d), (e) and (f) in Fig.2 because both ISRs are properly satisfied at these values and the experimental peak strength positions around 5 and 15 MeV regions are reproduced at the deformation region. For a reference, according to the RMF,  $^{26}\text{Mg}$  may have coexistent shapes,  $\beta_2=0.296$  and  $\beta_2=-0.261$  [20].

In Figs. 3 and 4, we show the  $GT(-)$  strength of  $^{76}\text{Ge}$  as a function of the excitation energy  $E_{ex}$  w.r.t. the ground state of  $^{76}\text{Ge}$ . The uppermost two panels are the experimental data from the  $^{76}\text{Ge}(p,n)^{76}\text{As}$  reaction at 134.4MeV [22], which show also a strong GT state peak around 14 MeV. Fig. 3 represent the calculated GT strength with prolate shapes,  $\beta_2 = 0 \sim 0.3$ , and Fig. 4 are for oblate shapes,  $\beta_2 = -0.1 \sim -0.3$ . Similarly to the Figs. 1 and 2, the GT strength distributions are widely scattered due to deformation. In specific, results for the  $\beta_2 = 0.3$ , in which the ISR I and II are almost satisfied, show reasonable results compared with the experimental data, whose  $\beta_2$  value is more or less consistent with the value calculated by RMF, 0.157 [20]. In particular, results by the value nicely reproduce the peak on the high-lying excited states around 14 MeV.

The GT strength,  $B(GT^-)$ , on  $^{82}\text{Se}$  is presented, in Fig. 5, as a function of the excitation energy  $E_{ex}$  w.r.t. the ground state of  $^{82}\text{Se}$  for  $\beta_2 = 0 \sim \pm 0.2$ . The uppermost panel of Fig. 5 is the experimental data from the  $^{82}\text{Se}(p,n)^{82}\text{Br}$  reaction at 134.4MeV [22]. In specific, the strong strength on the high-lying excited GT state around 12MeV is more or less reproduced by the  $\beta_2 = 0.145$  at (d) panel. For a reference, the  $\beta_2$  value from the RMF is 0.133 [20]. Our theoretical calculations address a possibility of another peak around 16 MeV.

The forward GT amplitudes  $X_{\alpha\alpha''\beta\beta'',K}$  for three highest GT transition peaks at 7.51, 12.29 and 15.78 MeV in (d) panel of Fig.5 are shown in Fig.6. Main transitions turn out to come from the  $(4311/2) \rightarrow (4311/2)$ ,  $(3101/2) \rightarrow (3101/2)$  and  $(3011/2) \rightarrow (3011/2)$ , and  $(4049/2) \rightarrow (4049/2)$  transition around the Fermi surface, respectively. They are thought to result from the 2p-2h configuration mixing stemming from the deformation around the Fermi surface.

Figs. 7 and 8 show the  $GT(\mp)$  strength on  $^{90}\text{Zr}$  as a function of the excitation energy  $E_{ex}$  w.r.t.  $^{90}\text{Zr}$ . The uppermost panels stand for the experimental data on  $GT(-)$  and  $GT(+)$  deduced from the  $^{90}\text{Zr}(p,n)^{90}\text{Nb}$  reaction  $^{90}\text{Zr}(n,p)^{90}\text{Y}$  at 293 MeV [23], respectively. Results in panels (c)~(e) are the results by the DQRPA for the different  $\beta_2$  values. For a reference, we show results by the spherical QRPA in each panel (b). The ISR I and II seem to be almost satisfied at  $\beta_2 = 0.1$  for both  $B(GT(\mp))$ . It means that the  $^{90}\text{Zr}$  is thought to be near to a spherical shape, *i.e.* slightly deformed. If we recollect that the experimental  $GT$  strength on the high-lying states beyond 30 MeV actually includes the contribution by the isovector spin monopole (IVSM) [23] which is not considered in the present calculation, our DQRPA results are well matched with the data compared with those by the DQRPA with  $\beta_2 = 0$ . Since our DQRPA is based on the deformation, the use of  $\beta_2 = 0$  may not be proper treatment. One more interesting point is that slightly deformed nuclei, such as  $^{90}\text{Zr}$ , did not show the high-lying  $GT(-)$  excited states appeared on  $^{76}\text{Ge}$  and  $^{82}\text{Se}$ . The high-lying states at the  $GT(+)$  transition is also neatly explained as shown at (d) in Fig. 8.

Fig. 9 show the  $GT$  strength of  $^{92}\text{Zr}$  as a function of the excitation energy  $E_{ex}$  w.r.t. the ground state of  $^{92}\text{Zr}$ . The uppermost panel (a) of Fig. 11 represent the experimental  $B(GT^-)$  values extracted from  $^{92}\text{Zr}(p,n)^{92}\text{Nb}$  reaction at 26 MeV, which is too lower to expect high-lying excited states. Excitation energies observed in this reaction are below 7 MeV. Panels (b) and (c) are the our results for  $\beta_2 = 0$  and 0.1. Results by  $\beta_2 = 0.1$ , which look like more reasonable than  $\beta_2 = 0$ , predict another peak around 8 MeV.

#### IV. SUMMARY AND CONCLUSION

To describe deformed nuclei, we performed the deformed axially symmetric Woods-Saxon potential, the deformed BCS, and the deformed QRPA with realistic two-body interaction calculated by Brueckner G-matrix based on Bonn CD potential. Results of the Gamow-Teller strength,  $B(GT\pm)$ , for  $^{26}\text{Mg}$ ,  $^{76}\text{Ge}$ ,  $^{82}\text{Se}$ ,  $^{90}\text{Zr}$ , and  $^{92}\text{Zr}$  show that the deformation effect leads to a fragmentation of the  $GT$  strength into high-lying  $GT$  excited states, in specific, on  $^{76}\text{Ge}$  and  $^{82}\text{Se}$  which  $GT$  data are discovered at recent charge exchange reaction experiments. Those states are properly explained by the deformation effects. More systematic analysis of deformed nuclei are under progress by including light nuclei characterized by the shell evolution or the inversion island.

These high-lying excited GT states may affect seriously relevant nuclear reactions, in specific, for neutrino-induced reactions, exploited in the nucleosynthesis because the emitted neutrinos from the proto-neutron star may have a high energy tail up to tens of MeV energy range. Since the experiments relate to the neutrino reaction on such a high energy would be a very challenging task in the present neutrino factories, the extraction of the high-lying GT states from charge exchange reactions could be very useful for understanding the neutrino reaction in the cosmos, if we recollect that the GT transitions are main components for the neutrino-induced reaction.

### Acknowledgement

This work was supported by the National Research Foundation of Korea (C00020, 2011-0015467, 2011-0003188).

### References

- 
- [1] T. Hayakawa, N. Iwamoto, T. Shizuma, T. Kajino, H. Umeda, and K. Nomoto, Phys. Rev. Lett. **93**, 161102 (2004).
  - [2] A. Heger, E. Kolbe, W.C. Haxton, K. Langanke, G. Martinez-Pinedo and S.E. Woosley, Phys. Lett. B **606**, 258 (2005).
  - [3] Myung-Ki Cheoun, Eunja Ha, T. Hayakawa, T. Kajino and S. Chiba, Phys. Rev. C **82**, 035504 (2010).
  - [4] Myung-Ki Cheoun, Eunja Ha, T. Hayakawa, Satoshi Chiba, Ko Nakamura, Toshitaka Kajino, Grant J. Mathews, arXiv:1108.4229 [nucl-th], (2011).
  - [5] P. Haensel and J. L. Zdunik, Nucl. Phys. (Proc. Suppl.) **B 24**, 139 (1991).
  - [6] F. Simkovic, L. Pacearescu, and A. Faessler, Nucl. Phys. **A 733**, 321 (2004).
  - [7] M. S. Yousef, V. Rodin, A. Faessler, and F. Simkovic, Phys. Rev. C **79**, 014314 (2009).
  - [8] M. K. Cheoun, A. Bobyk, Amand Faessler, F. Simkovic and G. Teneva, Nucl. Phys. **A 561**, 74 (1993) ; Nucl. Phys. **A 564**, 329 (1993); M. K. Cheoun, G. Teneva and Amand Faessler,



- Prog. Part. Nucl. Phys. **32**, 315 (1994) ; M. K. Cheoun, G. Teneva and Amand Faessler, Nucl. Phys. **A 587**, 301 (1995).
- [9] Myung-Ki Cheoun, Eunja Ha, K. S. Kim, and Toshitaka Kajino, J. Phys. **G 37**, 055101 (2010).
  - [10] M. Baranger, Phys. Rev. **130**, 1244 (1963).
  - [11] P. Ring, Y. K. Gambhir, and G. A. Lalazissis, Comput. Phys. Commun. **105**, 77 (1997).
  - [12] K. Blaum, Phys. Rep. **425**, 1 (2006).
  - [13] G. Bollen *et al.*, Nucl. Inst. and Method in Phys. Res. Sec. **A 368**, 675 (1997).
  - [14] K. Holinde, Phys. Rep. **68**, 121 (1981).
  - [15] T. Otsuka, Toshio Suzuki, Rintaro Fujimoto, Hubert Grawe, and Yoshinori Akaishi, Phys. Rev. Lett. **95**, 232502 (2005).
  - [16] T. Otsuka, Toshio Suzuki, Michio Honma, Yutaka Utsuno, Naofumi Tsunoda, Koshiroh Tsukiyama, and Morten Hjorth-Jensen, Phys. Rev. Lett. **104**, 012501 (2010).
  - [17] S. G. Nilsson and I. Ragnarsson, *Shapes and Shells in Nuclear Structure* (Cambridge University Press, Cambridge, UK, 1995)
  - [18] K. Hagino, N. W. Lwin, and M. Yamagami, Phys. Rev. C **74**, 017310 (2006).
  - [19] P. Raghavan, At. data Nucl. Data tables **42**, 189(1989).
  - [20] G. A. Lalazissis, S. Raman, P. Ring, At. Data and Nucl. Data tables **71**, 1-40 (1999).
  - [21] R. G. Zegers, *et al.*, Phys. Rev. C **74**, 024309 (2006).
  - [22] R. Madey, *et al.*, Phys. Rev. C **40**, 540 (1989).
  - [23] K. Yako, *et al.*, Phys. Lett. B **615**, 193 (2005).
  - [24] S. M. Grimes, *et al.*, Phys. Rev. C **53**, 2709 (1996).

TABLE I: Deformation parameters  $\beta_2$  and empirical (theoretical) pairing gap parameters  $\Delta_{\text{em}}^{\text{p,n}}$  ( $\Delta_{\text{th}}^{\text{p,n}}$ ) used in this work. The ISR in the last column denotes the Ikeda sum rules I (Eq.(34)) and II (Eq.(33)) as percentage ratios to  $3(N - Z)$ . The particle-particle(particle-hole) strength parameters are exploited as  $g_{\text{pp}} = 1.0(g_{\text{ph}} = 1.0)$  for all nuclei.

nucleus	$\beta_2$	$\Delta_{\text{em}}^{\text{p}}$ (MeV)	$\Delta_{\text{th}}^{\text{p}}$ (MeV)	$\Delta_{\text{em}}^{\text{n}}$ (MeV)	$\Delta_{\text{th}}^{\text{n}}$ (MeV)	ISR I, II(%)
$^{26}\text{Mg}$	0.0		2.342		1.909	127.62, 46.62
	0.1		2.331		1.907	138.56, 31.56
	0.2		2.349		1.905	139.89, 31.7
	0.3		2.348		1.907	123.83, 30.84
	-0.1	2.314	2.327	1.890	1.921	120.00, 50.54
	-0.2		2.342		1.906	109.44, 60.6
	-0.3		2.345		1.919	104.15, 74.12
	-0.4		2.333		1.898	97.70, 83.13
	-0.5		2.340		1.909	97.09, 82.26
$^{76}\text{Ge}$	0.0		1.581		1.536	88.40, 77.44
	0.1		1.575		1.538	84.22, 77.34
	0.2		1.578		1.540	88.35, 77.96
	0.3	1.561	1.562	1.535	1.537	88.67, 74.55
	-0.1		1.578		1.542	96.42, 84.38
	-0.2		1.561		1.549	94.63, 86.63
	-0.3		1.566		1.562	92.25, 88.11
$^{82}\text{Se}$	0.0		1.595		1.546	95.61, 84.20
	0.1		1.502		1.579	92.82, 83.46
	0.2	1.409	1.419	1.544	1.547	89.11, 80.34
	-0.1		1.410		1.564	101.14, 88.70
	-0.2		1.568		1.549	99.15, 90.03
$^{90}\text{Zr}$	0.0		1.458		1.711	110.76, 89.42
	0.1	1.247	1.267	1.705	1.713	94.61, 80.50
	-0.1		1.269		1.714	107.15, 79.29
$^{92}\text{Zr}$	0.0		1.467		0.849	104.39, 91.16
	0.1	1.357	1.378	0.841	0.847	104.30, 86.38

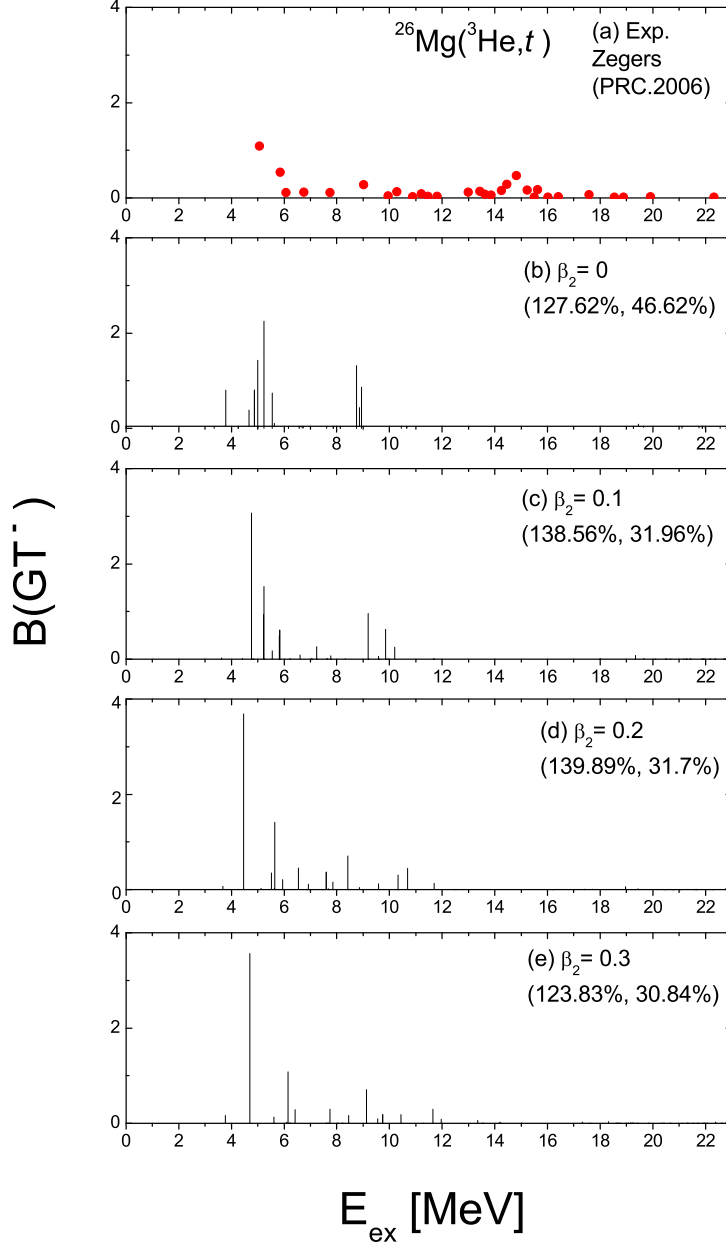


FIG. 1: (Color online) Gamow-Teller strength distributions,  $B(GT)$ , on  $^{26}\text{Mg}$  as a function of the excitation energy  $E_{ex}$  w.r.t. the ground state of  $^{26}\text{Mg}$ . Experimental data denoted as filled (red) points in the uppermost panels are deduced from the  $^{26}\text{Mg}(^3\text{He}, t)$  reaction at 140 MeV/nucleon [21]. In each panel, we indicate  $\beta_2$  and results of ISR as (ISR I, ISR II) which correspond to Eq. (34) and Eq. (33), respectively.

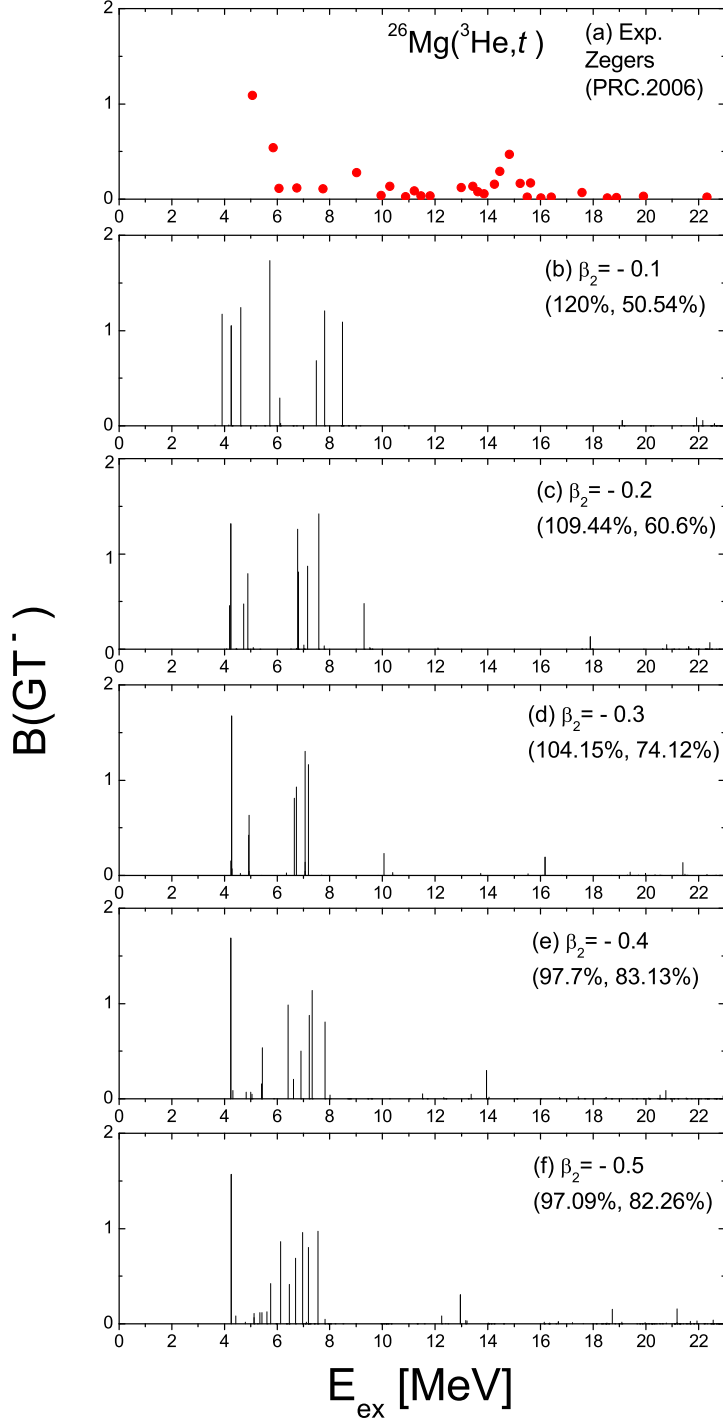


FIG. 2: (Color online) The same as in Fig. 1, but for an oblate shape,  $\beta_2 = -0.1 \sim -0.5$ .

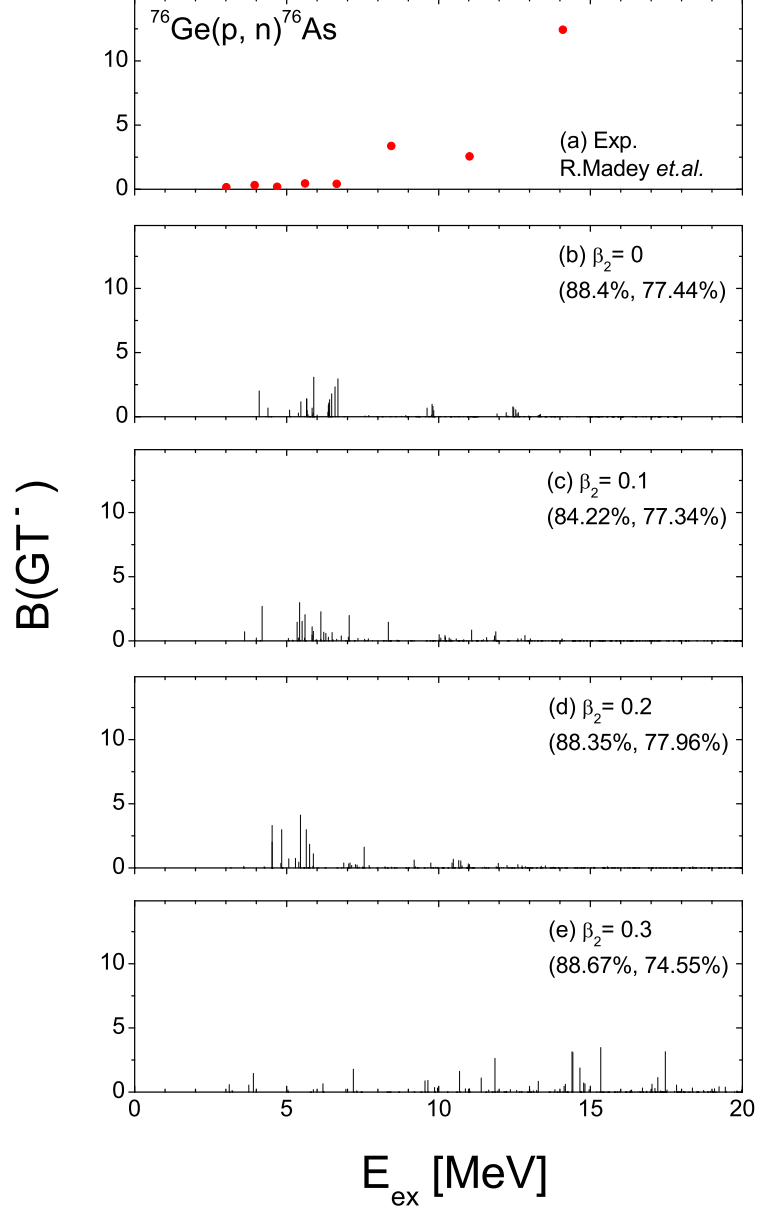


FIG. 3: (Color online) Gamow-Teller strength distribution  $B(GT^-)$  on  $^{76}\text{Ge}$  as a function of the excitation energy  $E_{ex}$  w.r.t. the ground state of  $^{76}\text{Ge}$ . Experimental data denoted as filled (red) points in the uppermost panels are deduced from the  $^{76}\text{Ge}(p,n)$  reaction at 134.4 MeV [22]. In each panel, we indicate  $\beta_2$  and results of ISR as (ISR I, ISR II) which correspond to Eq. (34) and Eq. (33), respectively.

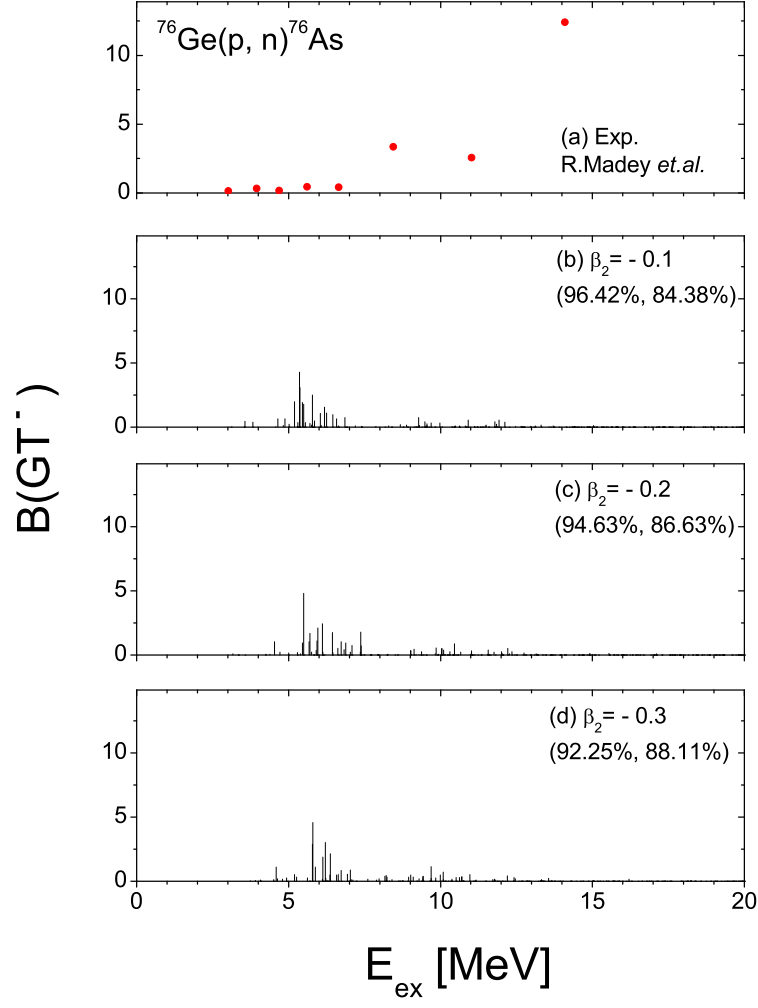


FIG. 4: (Color online) The same as in Fig. 3, but for an oblate shape,  $\beta_2 = -0.1 \sim -0.3$ .

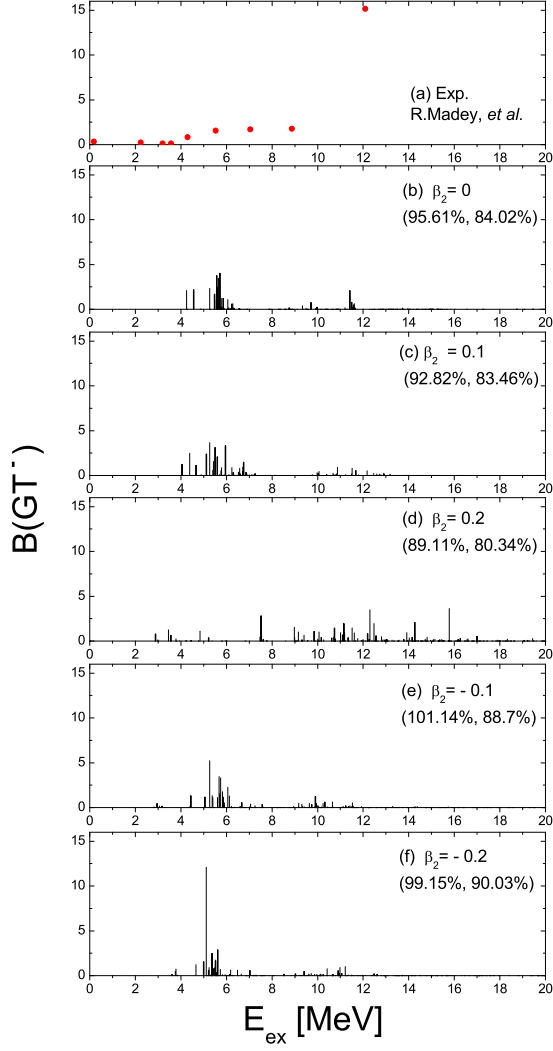


FIG. 5: (Color online) Gamow-Teller strength distribution  $B(GT^-)$  on  $^{82}\text{Se}$  as a function of the excitation energy  $E_{ex}$  w.r.t. the ground state of  $^{82}\text{Se}$ . Experimental data denoted as filled (red) points in the uppermost panels are deduced from the  $^{82}\text{Se}(p,n)$  reaction at 134.4 MeV [22]. In each panel, we indicate  $\beta_2$  and results of ISR as (ISR I, ISR II) which correspond to Eq. (34) and Eq. (33), respectively.

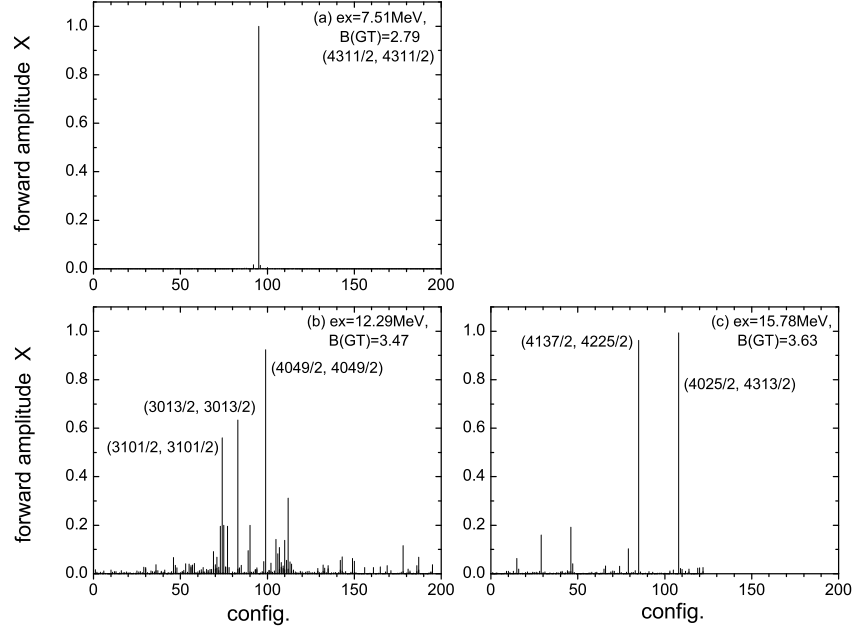


FIG. 6: Forward amplitudes  $X$  of the three highest GT strengths in (d) panel of Fig.5 at 7.51, 12.29 and 15.78 MeV w.r.t. the ground state of  $^{82}\text{Se}$ , which are presented for each GT transition configuration. Transition  $(4\ 3\ 1\ 1/2, 4\ 3\ 1\ 1/2)$  is the only physical component to the GT state at 7.51 MeV, and  $(3\ 1\ 0\ 1/2, 3\ 1\ 0\ 1/2)$  and  $(3\ 0\ 1\ 1/2, 3\ 0\ 1\ 1/2)$  transitions are main components for the GT state at 12.29, while transition  $(4\ 0\ 4\ 9/2, 4\ 0\ 4\ 9/2)$  is the main transition to the GT state at 15.78 MeV .



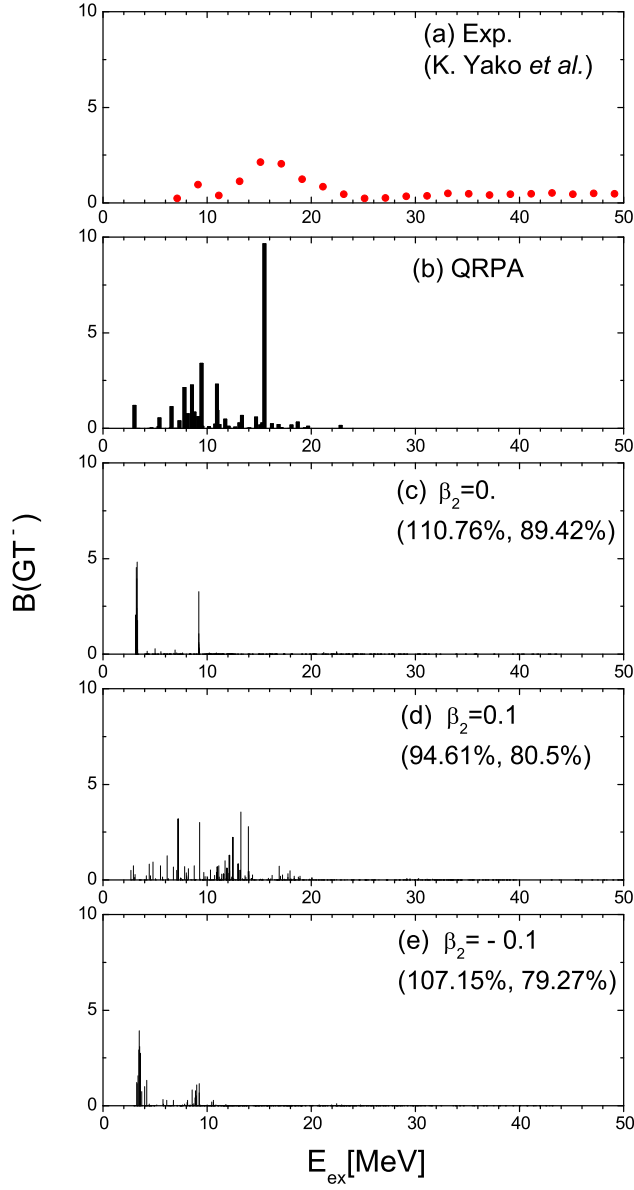


FIG. 7: (Color online) Gamow-Teller strength distribution  $B(GT^-)$  on  $^{90}\text{Zr}$  as a function of the excitation energy  $E_{ex}$  w.r.t. the ground state of  $^{90}\text{Zr}$ . Experimental data denoted as filled (red) points in the uppermost panels are deduced from the  $^{90}\text{Zr}(p,n)$  reaction at 293 MeV [23]. In each panel, we indicate  $\beta_2$  and results of ISR as (ISR I, ISR II) which correspond to Eq. (34) and Eq. (33), respectively.

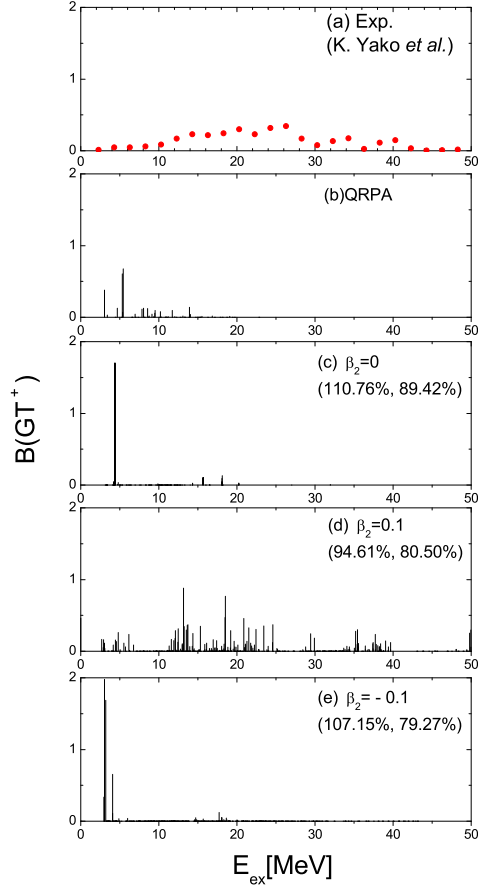


FIG. 8: (Color online) Gamow-Teller strength distribution  $B(GT^+)$  on  $^{90}\text{Zr}$  as a function of the excitation energy  $E_{ex}$  w.r.t. the ground state of  $^{90}\text{Zr}$ . The filled (red) circles in the uppermost panels are deduced from the  $^{90}\text{Zr}(n,p)$  reaction at 293MeV [23]. In each panel, we indicate  $\beta_2$  and results of ISR as (ISR I, ISR II) which correspond Eq. (34) and Eq. (33), respectively.

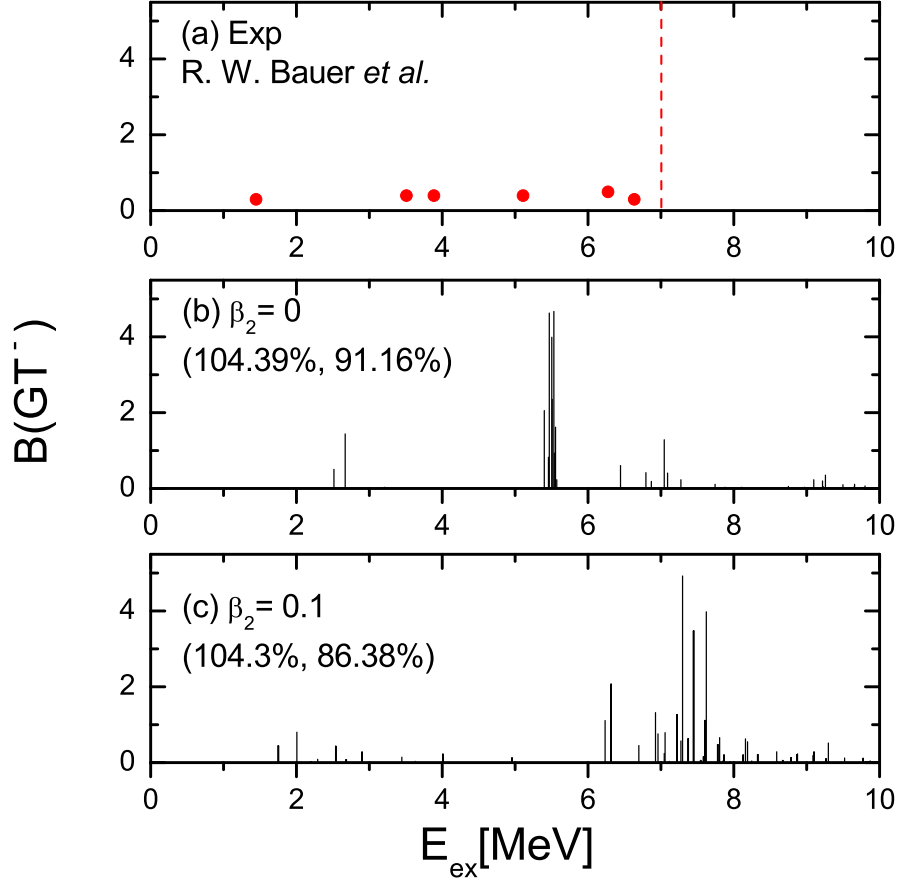


FIG. 9: (Color online) Gamow-Teller strength distribution  $B(GT^-)$  on  $^{92}\text{Zr}$  as a function of the excitation energy  $E_{\text{ex}}$  w.r.t. the ground state of  $^{92}\text{Zr}$ . Experimental data denoted as filled (red) points in the uppermost panels are deduced from the  $^{92}\text{Zr}(n,p)$  reaction at 26 MeV [24]. In each panel, we indicate  $\beta_2$  and results of ISR as (ISR I, ISR II) which correspond to Eq. (34) and Eq. (33), respectively.